EMI Prediction of Switching Converters

EMI Prediction of Switching Converters

Riccardo Trinchero, *Student Member, IEEE,* Igor S. Stievano, *Senior Member, IEEE,*
Flavio G. Canavero, *Fellow, IEEE*

***Abstract*—This paper addresses the simulation of the conducted electromagnetic interference produced by circuits with periodically switching elements. The proposed method allows for the computation of their steady-state responses by means of augmented linear time-invariant equivalents built from circuit inspection only, and standard tools for circuit analysis. The approach is demonstrated on a real dc-dc boost converter by comparing simulation results with real measurements.**

***Index Terms*—Boost converter, differential mode (DM), electromagnetic interference (EMI), switched circuits, time-frequency analysis.**

I. Introduction

Nowadays, switching power converters are massively used in electronic equipment and appliances. Due to their switching activity, these circuits represent the typical sources of the conducted electromagnetic interference (EMI) cluttering the power distribution network. Thus, their characterization is essential in order to understand and control their behavior, and comply with EMC regulations for conducted emissions (CE). Numerical simulation is the key tool in the early design phase to predict the generated electromagnetic noise and to carry out a systematic assessment of alternative design strategies for EMI suppression (e.g., see [1], [2]).

The classical approach to CE prediction is via time-domain simulation and the Fourier transform [3], [4]. In spite of its simplicity and effectiveness, this solution requires long simulation times to achieve accurate results and to avoid numerical integration errors. As an alternative, direct frequency-domain methods have been proposed in the literature ([2], [5], [6], [7] represent a sample of significant state-of-the-art contributions). Current techniques make use of simplifications to suppress the time-varying nature of the switches and to replace the original circuit with a linear time-invariant (LTI) surrogate, which however may lead to inaccuracies and unexpected behavior when the device operating condition is varied. The typical example is provided by a switching converter connected to the supply main via a suitably designed filter. It is worth noticing that for the case of time-varying circuits, the latter situation is similar to the one occurring when a small-signal LTI equivalent is used to predict the large-signal behavior of a nonlinear device.

To overcome the above limitations, this paper suggests an alternative frequency-domain solution to EMI prediction. The method is based on the well established theory of periodically switched linear (PSL) systems (e.g., see [8], [9], [10]). This approach provides a novel tool for accurate EMI prediction based on the simulation of a systematic augmentation of the original switching circuit, and allows to readily explain the mechanism of the generation of EMI disturbances. The validation of the proposed methodology is performed on a dc-dc boost converter, whose measured CE are excellently predicted by the augmented circuit.

R. Trinchero, I.S. Stievano and F. G. Canavero are with the Department of Electronics and Telecommunications, Politecnico di Torino, Corso Duca degli Abruzzi, 24, 10129, Torino, Italy, e-mail: {riccardo.trinchero,igor.stievano, flavio.canavero}@polito.it.

II. Harmonic generation in switching circuits

This section focuses on the discussion of the key underlying features of the steady-state responses of a switching circuit. For the sake of illustration, the schematic of Fig. 1 is considered. It provides a simple example that consists of the interconnection of both classical LTI and switched elements, and that exhibits the typical behavior of this class of circuits as shown by the curves of Fig. 2.

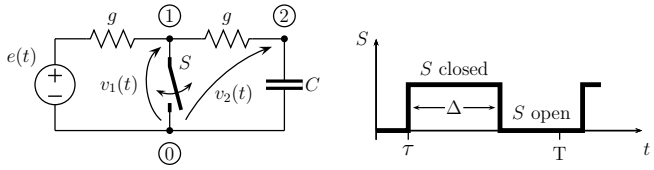

Figure 1. Example test case used to illustrate the proposed modeling approach (left panel). The circuit is excited by the source $e(t)$ and contains a generic switching element S characterized in the right panel by its switching function (T is the switching period, τ the closure instant and the duty cycle is $D = \Delta/T$.)

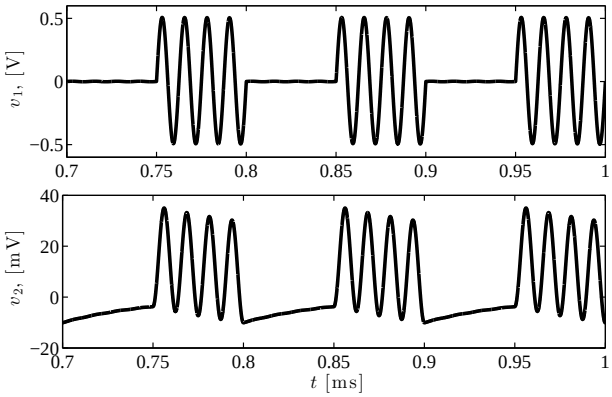

Figure 2. Steady-state response of the voltages $v_1(t)$ and $v_2(t)$ of the circuit of Fig. 1 to a sinusoidal excitation $e(t) = E_0 \sin(\omega_0 t)$, where $E_0 = 1\,\mathrm{V}$ and $f_0 = 80\,kHz$ ($\omega_0 = 2\pi f_0$). The remaining parameters take the following values: $g = 1/50\,\mathrm{S}$, $C = 1\,\mu\mathrm{F}$, and the switching frequency $f_c = 1/T = 10\,\mathrm{kHz}$.

The waveshapes of Fig. 2 clearly highlight that a generic switched circuit behaves analogously to an amplitude modulator, where the carrier is the excitation source (a sinusoidal waveform in this example) and the modulation signal is the

square wave defining the periodic activity of the switch (see Fig. 1). Of course, reactive elements (e.g., the capacitor of the example) unavoidably introduce additional dynamic effects as shown in the response v_2 of Fig. 2. This simple interpretation allows us to justify the behavior of switching circuits in both the time- and the frequency-domains. In fact, the circuit response to a single tone (i.e., a sinusoidal signal of angular frequency ω_0) modulated by the periodic activity of the switch element (i.e., a square wave signal characterized by an infinite number of harmonics, whose fundamental angular frequency is $\omega_c = 2\pi/T$) leads to a rich spectrum with many spikes centered on the carrier frequency and located at $\omega_0 \pm n\omega_c$, $n = 0, 1, 2, \ldots$. The above observation, that explains the key differences between LTI and PSL elements, is graphically illustrated in Fig. 3.

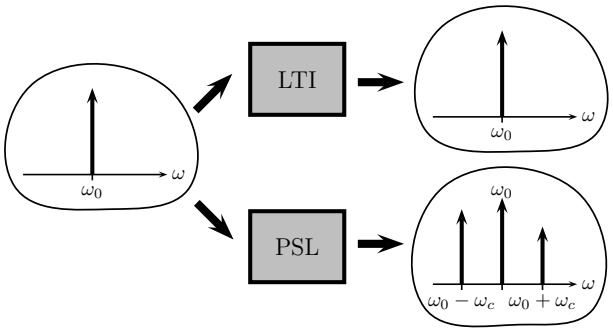

Figure 3. Graphical explanation of the response of LTI and PSL elements to a single tone excitation (see text for details).

The mathematical theory of linear periodic time-varying systems confirms, with a more rigorous mathematical apparatus, the qualitative behavior discussed above and suggests to approximating the steady-state response of a switched circuit in terms of a truncated harmonic expansion (e.g., see [9], [10], [11] and references therein). As an example, for the voltage $v_1(t)$ and a single tone excitation $e(t) = E_0 \exp(j\omega_0 t)$, the above approximation can be written:

$$v_1(t) \approx \sum_{n=-N}^{+N} V_{1,n} \exp(j\omega_0 t) \exp(jn\omega_c t), \qquad (1)$$

where $\omega_c = 2\pi f_c$ refers to the periodic switching, ω_0 represents the sinusoidal excitation of the circuit, and $V_{1,n}$ are the Fourier coefficients of the harmonics of voltage v_1. The same approximation holds for all the other voltage and current variables. For the case of a sinusoidal excitation, (1) can be readily modified by accounting for both the two frequency tones located at $\omega = \pm\omega_0$ (i.e. $E_0 \sin(\omega_0 t) = E_0(\exp(j\omega_0 t) - \exp(-j\omega_0 t))/2j$).

III. Augmented characteristics and steady-state solution

This section collects the basic steps of the proposed simulation method for the steady-state analysis of a PSL circuit. The following reasoning is based on a suitable interpretation of the harmonic coefficients defining the circuit response (i.e., $V_{1,n}$ of (1)) in terms of new variables of an augmented LTI circuit, that can be solved directly in the frequency-domain via standard tools for circuit analysis.

The method can be decomposed into the following two steps: generate the augmented LTI characteristics of all the circuit elements (see subsections A and B below) and obtain the steady-state solution of the original circuit in terms of the solution of an augmented LTI nodal equation (subsection C).

A. Characteristics of LTI Elements

For notational convenience, a generic two-terminal element with the associated voltage $v(t)$ and current $i(t)$ variables defined with passive sign convention is assumed. The electrical variables are represented by means of their corresponding Fourier transforms and are approximated by means of a truncated series of delta functions (e.g., $V(\omega) = \mathcal{F}\{v(t)\} \approx \sum_{n=-N}^{+N} V_n \delta(\omega - n\omega_c - \omega_0)$).

For the case of a simple resistor, the relation between its current and voltage harmonics turns out to be frequency independent and written as:

$$I_n = V_n/R = GV_n, \quad n = -N, \ldots, 0, \ldots, N. \qquad (2)$$

For the case of dynamic LTI elements, such as a capacitor, the constitutive relation becomes

$$I_n = j(\omega_0 + n\omega_c)CV_n, \quad n = -N, \ldots, 0, \ldots, N, \qquad (3)$$

and similarly for an inductor.

B. Characteristics of Switching Elements

When dealing with a switch, the computation requires additional effort. A generic switch, like S of Fig. 1, is assumed to be described by a two-terminal element that consists of the series connection of an ideal switching element and of a finite series resistance R_{ON}, leading to the following constitutive relation:

$$I_n = \sum_{m+l=n} Y_l V_m, \quad n, m = -N, \ldots, 0, \ldots, N, \qquad (4)$$

where the coefficients Y_l are defined by closed-form analytical formula that can be easily computed from the information of the switching operation (i.e., the quantities defined on the right-hand-side panel of Fig. 1). Intuitively, (4) is justified by the PSL branch of Fig. 3 and is more deeply discussed in [12], where the Y_l coefficients are derived and shown to be

$$Y_l = f_c \frac{1}{R_{ON}} \frac{\exp(-jl\omega_c\tau) - \exp(-jl\omega_c(\tau + DT))}{jl\omega_c}, \qquad (5)$$

where the parameters of the switching function are defined in the right-hand-side panel of Fig. 1.

It is relevant to remark that (4) can be used to approximate the behavior of any binary switching device in a PSL circuit, like diodes or MOS transistors. In addition, (4) highlights that the switch leads to a fully coupled relationship involving the combination of all the different harmonics, as opposed to any LTI components characterized by single-frequency relationships (see (2), (3) and the upper branch of Fig. 3).

C. Augmented Circuit and Solution

Based on (2), (3) and (4), the constitutive relations of the elements of a generic switching circuit can be rewritten in a more compact form as follows:

$$\mathbf{I} = \mathbf{Y}\mathbf{V}, \tag{6}$$

where $\mathbf{V} = [V_{-N}, \ldots, V_0, \ldots, V_N]^T$ and $\mathbf{I} = [I_{-N}, \ldots, I_0, \ldots, I_N]^T$ are vectors filled by the harmonic coefficients defining the steady-state response of the corresponding variables. In turn, $\mathbf{Y}$ is interpreted as an admittance representation with size $(2N+1) \times (2N+1)$ and suitable coefficients. For classical LTI elements, (2) and (3) indicate that $\mathbf{Y}$ is a diagonal matrix. Conversely, switching elements defined by (4) yield a full matrix containing the coupling coefficients among the different harmonics of the voltage and current variables.

The most important outcome of the above interpretation is that each element of a switching circuit can be replaced by an augmented admittance block that can be combined with the others using the same topological structure of the original circuit. The augmented circuit is readily generated from circuit inspection only and can be solved via standard tools (such as the modified nodal method) via simple linear inversion. Finally, the steady-state response of the the PSL circuit can be reconstructed by means of expressions analogous to (1), where the spectral coefficients are the solutions of the augmented circuit.

As a first validation, the proposed approach is applied to the example of Fig. 1, for which an augmented model with expansion order $N = 50$ has been used. Fig. 4 shows the predicted spectrum of voltage v_2, compared with the Fourier transform of the circuit response obtained by time integration of the circuit ordinary differential equations (ODE). This comparison highlights the good accuracy and of the solution. In fact, the relative mean square error of the difference between the reference and the predicted time-domain steady-state responses is $< 0.05\%$. Also, the proposed method is very efficient, since the computation via the augmented circuit is $30\times$ faster than the ODE integration.

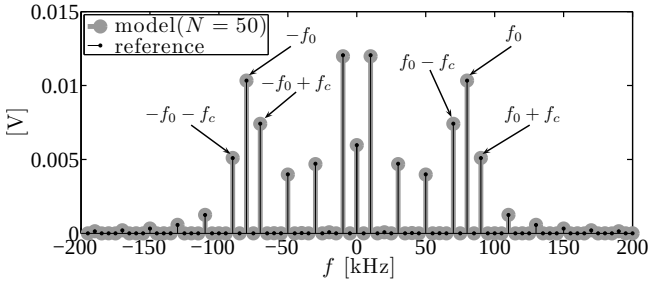

Figure 4. Frequency-domain spectrum of the voltage $v_2(t)$ of the example circuit of Fig. 1. The reference response (thin black lines) is compared with the solution of the augmented circuit with expansion order $N = 50$ (thick gray lines).

IV. Application test case

The proposed method is validated on a real test case involving a dc-dc boost power converter in the typical configuration of Fig. 5 and is used to estimate its differential mode (DM) noise EMI spectrum.

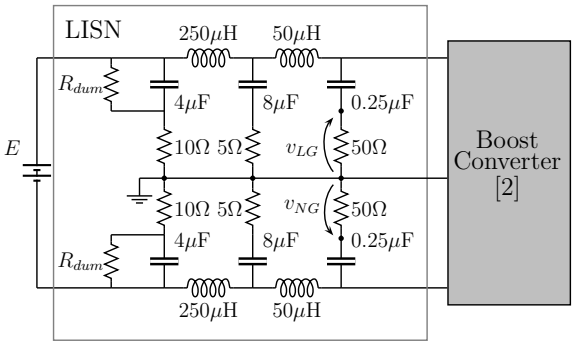

Figure 5. Setup for the simulation and measurements of the DM emissions of a switching power converter: the stabilization network (LISN) is detailed and the dc-dc boost circuit is given in [2].

The parameters and operating conditions defining this example test case are the following: the converter operates in continuous mode at $f_c = 40\,\text{kHz}$ with duty cycle $D = 45\%$; the input voltage $E = 20\,\text{V}$ is applied through the line impedance stabilization network (LISN). Additional details on this example test case and on the time-domain measurements carried out are provided in [2].

The DM noise voltage is detected through the LISN as the difference between the line-to-ground v_{LG} and the neutral-to-ground v_{NG} voltages:

$$v_{DM}(t) = \frac{v_{LG}(t) - v_{NG}(t)}{2}. \tag{7}$$

According to the procedure outlined in Section III, the augmented LTI equivalent built from the complete schematic of Fig. 5 is generated. For the boost circuit represented by the gray box of Fig. 5, all individual elements are used, and the diode and the MOS devices are suitably replaced by two periodic switches. According to the technical datasheets, the non-ideal behavior of both the MOS and the diode is provided by the inclusion of their own parasitic capacitances and switching misalignment. The reference results are represented by time-domain measurements performed on a circuit built according to the schematic of Fig. 5.

Fig. 6 shows the comparison between the reference and the predicted time-domain responses of the DM noise voltage $v_{DM}(t)$. From the curves of this figure, it is clear that the proposed method allows us to generate predictions with a tunable accuracy depending on the expansion order N. The bottom panel of Fig. 6 highlights that $N = 100$ is sufficient to describe the overall signature of the DM noise without the localized spikes. To achieve a better accuracy, the expansion order unavoidably needs to be increased to a much larger value (e.g., $N = 1000$). In the latter case, the agreement is excellent and the measured responses are very well reproduced by the prediction.

Similarly, Fig. 7 shows a comparison of the reference and predicted frequency-domain spectra of the DM noise, thus confirming the accuracy of the predicted responses in reproducing both the envelope and the notches of the reference

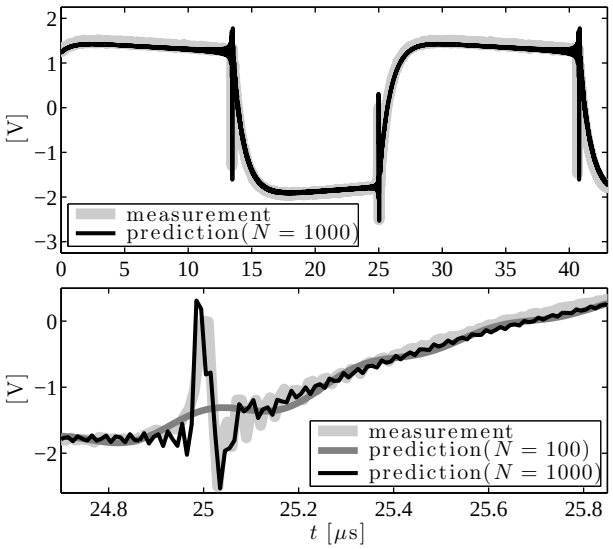

Figure 6. DM noise voltage $v_{DM}(t)$ of the example test case of Fig. 5. Light gray: measurement; dark gray: prediction ($N = 100$); black thin: prediction ($N = 1000$). The bottom panel represents an expansion of the time scale to demonstrate the need of higher-order harmonics for a full reconstruction of all details.

curve. From the curves in Fig. 7 it is even more evident that the expansion order should be large enough to cover the entire bandwidth required for the characterization of the conducted emissions spectrum (i.e., 150 kHz–30 MHz). Since the largest harmonic of the series expansion of (1) is located at $f_{\max} = f_0 + Nf_c$, for the boost example with a constant voltage excitation (i.e., $f_0 = 0$ Hz), the minimum number of harmonics spanning a 30 MHz bandwidth turns out to be $N \geq (30\,\text{MHz}/f_c = 750)$.

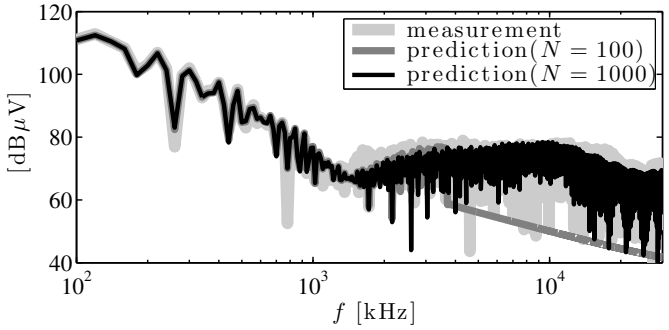

Figure 7. Frequency-domain spectrum of DM noise voltage $v_{DM}(t)$ for the example test case of Fig. 5. Light gray: measurement; dark gray: prediction ($N = 100$); black thin: prediction ($N = 1000$).

To conclude the comparison, Table I reports the efficiency and covered bandwidth of the proposed method, for an increasing size of the expansion order N. The numbers in the table, that are obtained by a MacBook Pro (Intel Core i5 running a@ 2.4 GHz, 4 GB RAM), highlight a reduced CPU time in generating the steady-state response of the example test circuit for any value of N. Even if a large expansion number is considered (i.e., $N = 1000$), the EMI prediction is always achieved in a reasonable amount of time.

Table I
EFFICIENCY AND COVERED BANDWIDTH FOR AN INCREASING NUMBER OF THE EXPANSION ORDER N (SEE TEXT FOR DETAILS).

N	10	100	500	1000
Cpu time	0.016 s	0.23 s	1.08 s	9.79 s
Bandwidth	366 kHz	3.66 MHz	18.31 MHz	36.63 MHz

V. CONCLUSIONS

This paper addressed the simulation of the steady-state response of a switching circuit with the aim of predicting its EMI disturbances propagating in the power distribution network. The proposed approach provides an alternative yet effective topological solution that is based on the generation of an augmented linear time-invariant equivalent. The solution of the above augmented network via standard tools (such as the classical nodal method) at a single frequency point allows us to compute the harmonic coefficients of the steady-state circuit response. The method is illustrated on a simple example and its feasibility and strength are demonstrated on a real dc-dc boost circuit. Predicted responses are compared with measured data, yielding remarkable accuracy and good simulation time reduction.

REFERENCES

[1] V. Tarateeraseth, S. Kye Yak, F.G. Canavero, R.W. Chang, “Systematic Electromagnetic Interference Filter Design Based on Information From In-Circuit Impedance Measurements”, IEEE Trans. on Electromagnetic Compatibility, Vol. 52, No. 3, pp. 588–598, Aug. 2010.

[2] V. Tarateeraseth, I.A. Maio, F.G. Canavero, “Assessment of Equivalent Noise Source Approach for EMI Simulations of Boost Converter.", Proc. of the *20th Int. Zurich Symposium on EMC*, pp. 353–356, Jan. 2009.

[3] X. Pei, Jian Xiong, Y. Kang, J. Chen, “Analysis and suppression of conducted EMI emission in PWM inverter", in Proc. of the *Int. Conf. IEMDC'03 on Electric Machines and Drives*, Vol. 3, pp. 1787–1792, June 2003.

[4] Y. Koyama, M. Tanaka, H. Akagi,“Modeling and analysis for simulation of common-mode noises produced by an inverter-driven air conditioner", in Proc. of *Int. Conf. on Power Electronics (IPEC)*, pp. 2877–2883, June 2010.

[5] Y. Liu, Kye Yak See; King-Jet Tseng, “Conducted EMI Prediction of the PFC Converter Including Nonlinear Behavior of Boost Inductor", IEEE Trans. on EMC, Vol. 55, No. 6, pp. 1107–1114, Dec. 2013.

[6] F. Yang, X. Ruan, Q. Ji; Z. Ye, “Input Differential-Mode EMI of CRM Boost PFC Converter", IEEE Trans. on Power Electronics, Vol. 28, No. 3, pp. 1177–1188, March 2013.

[7] R. Kahoul, Y. Azzouz, P. Marchal, B. Mazari, “New Behavioral Modeling for DC Motor Armatures Applied to Automotive EMC Characterization", IEEE Trans on EMC, Vol. 52, No. 4, pp. 888–901, Nov. 2010.

[8] L. A. Zadeh, “Frequency Analysis of Variable Networks”, Proceedings of the IRE, Vol. 38, No. 3, pp. 291–299, Mar. 1950.

[9] H. Sandberg, E. Mollerstedt, Bernhardsson, “Frequency-domain analysis of linear time-periodic systems", IEEE Trans. on Automatic Control, Vol. 50, No. 12, pp. 1971–1983, Dec. 2005.

[10] T.A.C.M. Claasen, W. F. G. Mecklenbrauker, “On stationary linear time-varying systems”, IEEE Trans. on Circuits and Systems, Vol. 29, No. 3, pp. 169–184, Mar. 1982.

[11] R. Trinchero, I. S. Stievano, F. G. Canavero, “Steady-State Response of Periodically Switched Linear Circuits via Augmented Time-Invariant Nodal Analysis", Journal of Electrical and Computer Engineering, Vol. 2014, pp. 1–11, 2014.

[12] R. Trinchero, I. S. Stievano, F. G. Canavero, “Steady-State Analysis of Switching Power Converters Via Augmented Time-Invariant Equivalents", IEEE Trans. on Power Electronics, Vol. 29, No. 11, pp. 5657–5661, Nov. 2014.